Frascati Physics Series Vol. XXI (2000), pp. 709–720
IX INT. CONF. ON CALORIMETRY IN PART. PHYS. - Annecy, Oct. 9-14, 2000

NEW TYPES OF LEAD TUNGSTATE CRYSTALS WITH HIGH LIGHT YIELD

R.H. Mao, G.H. Ren, D.Z. Shen, Z.W. Yin
Shanghai Institute of Ceramics, Shanghai 200050, P.R.C.
X.D. Qu, L.Y. Zhang, R.Y. Zhu
California Institute of Technology, Pasadena, CA 91125, U.S.A
S.P. Stoll, C.L. Woody
Brookhaven National Laboratory, Upton, NY 11973, U.S.A

ABSTRACT

Because of their high stopping power and fast scintillation, lead tungstate crystals have attracted much attention in the high energy physics and nuclear physics communities. The use of lead tungstate, however, is limited by its low light output. An effort has been made at the Shanghai Institute of Ceramics to improve this. The results indicate that up to a factor of ten increase in the light output, mainly in the microsecond decay component, may be achieved. The X-ray diffraction pattern, photo luminescence spectrum, light output, decay kinetics and transmittance spectrum of new samples are presented. Longitudinal uniformity of a sample of 22 radiation lengths is studied. Possible applications for calorimetry in high energy and nuclear physics experiments are discussed.

1 Introduction

In the last five years an extensive R&D program has been carried out by the Compact Muon Solenoid (CMS) experiment in developing lead tungstate ($PbWO_4$) crystals to be used in the Large Hadron Collider (LHC). As a result of this development program, a total of 11.2 m^3 large size (25 X_0) $PbWO_4$ crystals with fast scintillation light will be produced in Bogoroditsk Techno-Chemical Plant (BTCP) in Tulla, Russia, and in Shanghai Institute of Ceramics (SIC) in Shanghai, China. Because of this development, $PbWO_4$ crystal is now a mature material in market with low cost.

It, however, is interesting to note that the Y doped $PbWO_4$ crystals chosen by CMS have limited light output, about 10 p.e/MeV for full size samples measured with a photo multiplier (PMT) of bi-alkali cathode. This limits their application in areas other than high energy and nuclear physics. One approach to modify scintillation property of a material is altering crystal structure by changing growth parameter. Doping during crystal growth is another approach which may compensate structure defects, eliminate unwanted impurities and change scintillation properties. In developing BGO crystals for the L3 experiment, Eu doping was used at SIC to improve its radiation resistance [1)]. In developing CsI(Tl) crystals for the $BaBar$ and BELLE experiments, a special scavenger was used at SIC to remove oxygen contamination [2)]. Pentavalent (Nb) doping in $PbWO_4$ was first reported by Lecoq *et al.* to be effective in improving transmittance at 100 ppm level [3)]. Trivalent (La) doping was first reported by Kobayashi *et al.* to be effective in improving both the transmittance [4)] and the radiation hardness [5)]. Consequent studies on doping with various ions, such as La, Lu, Gd, Y and Nb, at optimized level were reported to be effective in improving transmittance as well as radiation hardness [6, 7)].

Early Glow Discharge Mass Spectroscopy (GDMS) analysis revealed that contaminations of certain cation, especially Mo, were responsible for the slow scintillation component in $PbWO_4$, as reported by Kobayashi *et al.* [8)] and Zhu *et al.* [9)]. On the other hand, Mo doping introduces a significant fraction of the slow component and thus increases the light output in $PbWO_4$ crystals. Following this line, $PbWO_4$ samples doped with various dopant were grown and were found with significant increase of light yield [10, 11)]. In this paper we present scintillation and other optical properties of $PbWO_4$ crystals doped with two special dopant A and B[1]. It is found

[1]Pending on patent application, the chemical nature of particular dopant is not released at present.

that light output of up to ten folds of that of the CMS Y doped $PbWO_4$ crystal, mainly in the microsecond decay component, can be achieved. $PbWO_4$ crystals of this type may find applications in high energy and nuclear physics experiments, such as crystal calorimeters in future electron linear colliders or in heavy ion colliders, where interaction cross-section allows an integration time of a few μs.

2 Samples

A total of ten samples, grown by a modified Bridgman method at SIC, were studied. Table 1 lists the dimension, dopant, peak of the photo luminescence and the sample delivery date. As a comparison, a standard CMS Y doped sample S762, which is a 23 cm long tapered from 2.2×2.2 cm^2 to 2.6×2.6 cm^2, is also listed in this table. Two different dopants (A and B) were introduced at different levels in the melt during growth.

Table 1: List of Samples Investigated in this Paper

ID	Dimension(cm)	λ_{pho} (nm)	Date
Samples Doped with Dopant A			
S25	$2.9 \times 9.5 \times 2.9$	570	4/23/1999
S27	$2.0 \times 12.0 \times 2.0$	570	4/26/2000
Z9	$2.0 \times 19.8 \times 2.0$	570	4/26/2000
Z14	$2.0 \times 17.9 \times 2.0$	570	7/21/2000
Z22	$2.0 \times 16.0 \times 2.0$	570	7/21/2000
Z23	$2.0 \times 9.7 \times 2.0$	570	7/21/2000
Z24	$2.0 \times 3.0 \times 2.0$	570	9/20/2000
Z25	$2.0 \times 12.0 \times 2.0$	570	9/20/2000
Samples Doped with Dopant B			
Z20	$2.0 \times 14.0 \times 2.0$	570	7/21/2000
Z21	$2.0 \times 10.3 \times 2.0$	570	7/21/2000
A Standard CMS Y Doped Sample			
S762	$2.2 \times 23.0 \times 2.6$	430	8/25/2000

All samples have rectangular shape with all surfaces polished. No further treatment, other than simple cleaning with alcohol, was carried out before measurements.

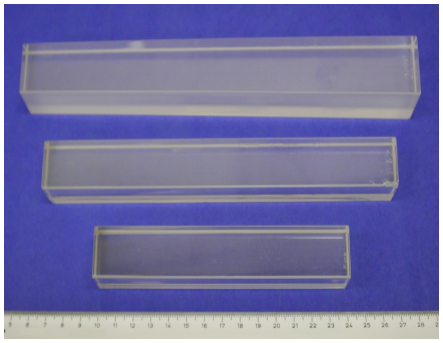

Figure 1: A photo showing, from top to bottom, a standard CMS Y doped sample S762, an A doped sample Z9 and a B doped sample Z20.

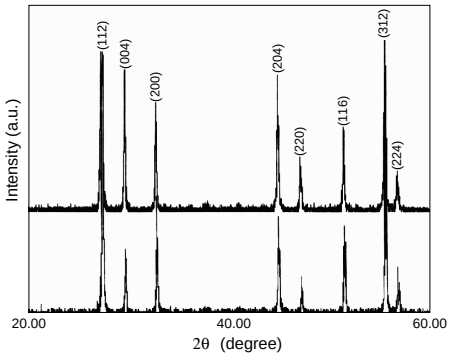

Figure 2: XRD patterns for samples Z24 and Z25.

The as-grown samples are transparent, colourless without visible defects, such as cracking, inclusions, scattering particles and growth striation. Figure 1 is a photo showing, from top to bottom, a standard CMS Y doped sample S762, an A doped sample Z9 and a B doped sample Z20.

Both A and B dopings do not change crystal structure. Figure 2 shows the X-ray diffraction (XRD) patterns measured at SIC. Two small blocks cut from samples Z24 and Z25 were grounded into powders, and the XRD spectra were taken by using a D/MAX-C diffractometer with a Cu target running at 40 kV, 30 A and 2 °/min. Both patterns match very well with standard power diffraction data of pure sheelite structure [12]. No other phase was observed.

3 Emission

Photo luminescence spectrum was measured by using a Hitachi F-4500 fluorescence spectrophotometer equipped with a red sensitive Hamamatsu PMT R928, which extends measurement range from 220 to 800 nm. Figure 3 shows a schematic of the setup, where the UV excitation light was shot to a bare surface of a sample and the photo luminescence, without passing through sample to avoid effect of self absorption, was measured by an R928 PMT through a monochromator. Figure 4 shows the photo luminescence spectra for an A doped sample Z24, a B doped sample Z20 and a

standard CMS Y doped sample S762. These spectra were corrected by the monochromator efficiency and the PMT quantum efficiency. The vertical axis refers to photon numbers, and its scale is arbitrary. As shown in Figure 4, both A and B doped samples have similar photo luminescence peaked at 570 nm, while that from sample S762 is peaked at 430 nm. This means that the scintillation of these new types of $PbWO_4$ crystals is in green, contrary to the blue of standard CMS Y doped $PbWO_4$ crystals.

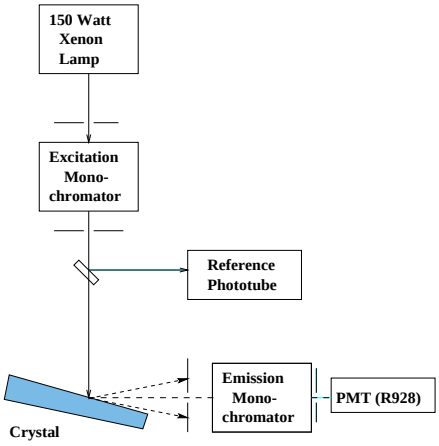

Figure 3: A schematic of setup used to measure photo luminescence.

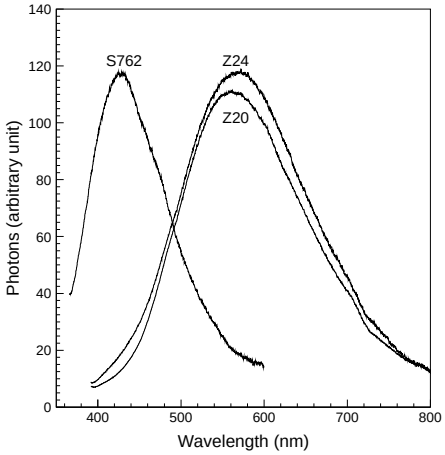

Figure 4: Photo luminescence spectra for samples Z24, Z20 and S762.

4 Light Output and Decay Kinetics

The scintillation light output was measured by using a Hamamatsu PMT R2059, which has a bialkali photo cathode and a quartz window. To study crystal uniformity measurements were carried out by coupling both the seed and the tail end of a sample to the PMT. A thin layer of Dow Corning 200 fluid, which has very good UV transmittance [13], was used between the sample and the PMT, while all other faces of the sample were wrapped with two layers of the Tyvek paper. A collimated ^{137}Cs source was used to excite the sample, shooting at the non coupling end of the sample. The scintillation light pulse collected by the PMT was integrated by a LeCroy 3001 QVT in the Q mode. A series of 8 integration gates, ranging from 35 to 4000 ns, was provided by a LeCroy 2323A programmable gate generator to measure the light output as

a function of integration time. The γ-ray peak was determined by a simple Gaussian fit, and was used to determine photoelectron numbers by using the single photoelectron peak. The measured photoelectron numbers can be converted to the photon yield of the sample by taking into account the quantum efficiency of the photocathode and the efficiency of the light collection.

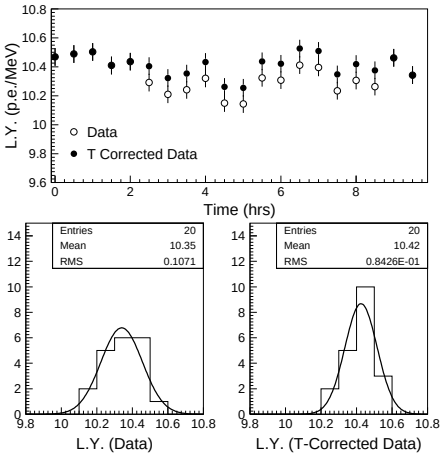

Figure 5: Light output measured by a PMT in 9 hours (top), and its distribution without (left bottom) and with (right bottom) temperature corrections.

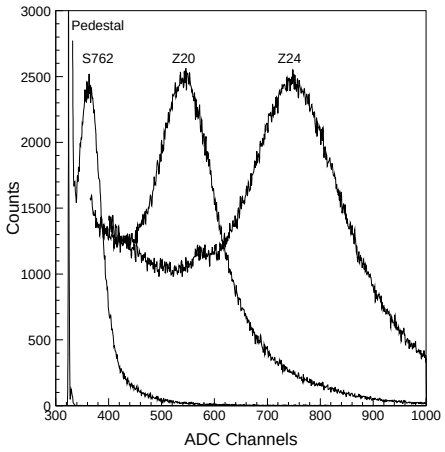

Figure 6: ^{137}Cs spectra integrated in 2 μs for samples Z24, Z20 and S762.

All measurement were carried out at the room temperature of 20 °C. Data were corrected by using the room temperature which has daily variations of up to 0.5 °C, despite central air condition of entire laboratory building and individual temperature adjustment and feedback in the room where measurement was carried out. This variation is significant since the light output of $PbWO_4$ crystals is known to have -2%/°C at room temperature. The systematic uncertainty of light output measurement, including temperature variation and operation uncertainties caused by mounting samples to the PMT, was estimated to be about 1%. With temperature corrections this uncertainty is reduced to 0.8%. The top plot in Figure 5 shows the repeated measurement of the light output for a sample in 9 hours. Two bottom plots in Figure 5 show raw (left) and temperature corrected (right) light output data and corresponding Gaussian fit. A precision of 1 and 0.8% were achieved for the light output measurement without and

with temperature corrections respectively.

Figure 6 shows ^{137}Cs spectra integrated in 2 μs from an A doped sample Z24, a B doped sample Z20 and a standard Y doped CMS $PbWO_4$ sample S762. Both A and B doped samples have significantly more light than CMS sample, and the A doped sample Z24 has more light than the B doped sample Z20, part of which can be explained by the small size of sample Z24.

Table 2: Summary of $PbWO_4$ Light Output (p.e/MeV)

Sample	Gate width (ns)					Fraction(%)	
ID	50	100	200	1,000	2,000	$\frac{50ns}{2\mu s}$	$\frac{100ns}{2\mu s}$
S25^s	10.2	14.8	22.3	49.2	55.4	18	27
S25^t	10.5	13.8	17.7	29.8	31.8	33	43
S27^s	11.3	15.2	20.4	40.5	46.1	25	33
S27^t	12.5	15.7	17.0	18.9	19.4	64	81
Z9^s	6.1	8.3	11.1	22.4	26.0	24	32
Z9^t	6.0	7.9	8.7	9.0	9.1	66	87
Z23^s	21.0	27.3	31.5	40.4	41.8	50	65
Z23^t	20.3	25.4	27.4	29.7	30.2	67	84
Z24^s	22.3	28.4	36.5	71.0	82.5	27	34
Z24^t	22.0	27.5	34.5	63.1	72.4	30	38
Z20^s	8.2	9.5	9.7	9.8	9.9	83	96
Z20^t	9.9	13.7	19.9	46.0	54.3	18	25
Z21^s	21.3	28.0	31.3	34.5	35.1	61	80
Z21^t	20.5	28.5	34.4	42.0	42.4	48	67
S762	9.3	10.3	10.4	10.4	10.4	89	99

^{s} represents sample's seed end coupled to the PMT.
^{t} represents sample's tail end coupled to the PMT.

Table 2 lists the light output integrated in five different gate widths for all $PbWO_4$ samples listed in Table 1. Also listed in the table is the ratio of light outputs between 50, 100 and 2,000 ns. Significant increase of light output, especially in slow scintillation component, is observed for samples doped with A and B. With light output measured as a function of integration time, the scintillation decay kinetics of

the samples was determined. Figure 7 shows a comparison of light outputs, in photoelectron per MeV, as a function of the integration time for samples Z24, Z20 and S762. The A and B doped samples have significantly increased slow component.

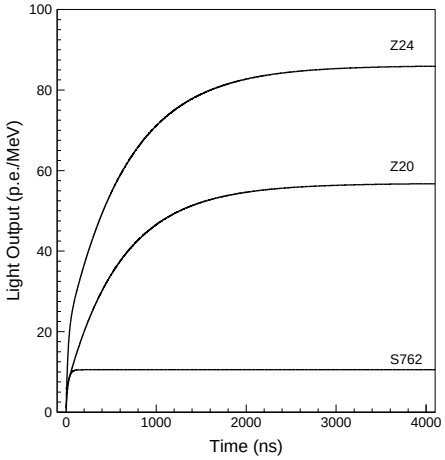

Figure 7: The light output is shown as a function of integration time for samples Z24, Z20 and S762.

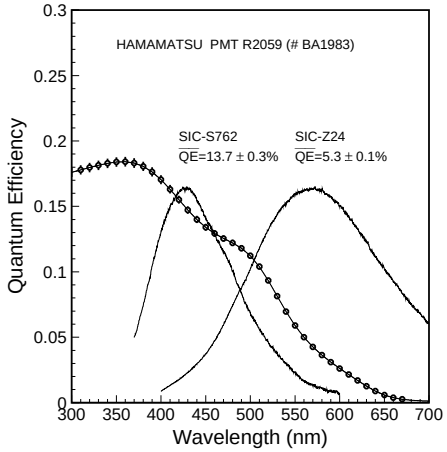

Figure 8: Quantum efficiency of R2059 PMT is ahown as function of wavelength together with emission spectra of A doped sample Z24 and Y doped sample S762.

On the face value of Table 2 and Figure 7, the A or B doped samples may provide photo electron yield of up to 5 to 8 times of that of the Y doped CMS crystal. To convert the measured photoelectron yield to the photon yield we measured emission weight quantum efficiency of the Hamamatsu R2059 PMT used in the measurement. Figure 8 shows distributions of the quantum efficiency of R2059 PMT and corresponding emission spectra for a CMS choice of Y doped $PbWO_4$ sample S762 and an A doped $PbWO_4$ sample Z24. The corresponding emission weighted quantum efficiencies are $(13.7 \pm 0.3)\%$ and $(5.3 \pm 0.1)\%$ respectively for S762 and Z24. The PMT response thus has a factor 2.6 difference for these two types of crystals. Calculation by using emission of a B doped sample shows consistent result. The light output of A or B doped samples in photon/MeV thus is 13 to 21 times of that of Y doped $PbWO_4$. This number, however, has not taken into account the difference of the light path or crystal size. Taking into account the difference of the light path, our estimation is

that up to a factor of ten increase in light output, mainly in μsec decay component, is expected for the A and B doped samples as compared to that of the standard Y doped CMS sample.

Reading Table 2 one also notices that the difference of the light output between the seed and the tail end coupled to the PMT for the same sample. This is caused by the variation of the emission spectrum along the crystal length and will be discussed in details in Section 6.

5 Longitudinal Transmittance

Longitudinal transmittance was measured by using a Hitachi U-3210 UV/visible spectrophotometer with double beam, double monochromator and a large sample compartment equipped with a custom Halon coated integrating sphere. The systematic uncertainty in repeated measurements of transmittance was approximately 0.3%. Figure 9 shows longitudinal transmittance spectra for an A doped sample Z24, a B doped sample Z21 and a CMS Y doped sample S762. While the transmittance of Z24 is the highest, that of S762 is the lowest. This is partly due to the difference of the path length: 3, 10 and 23 cm respectively for samples Z24, Z21 and S762. One also notes that transmittance of sample Z24 approaches the theoretical limit.

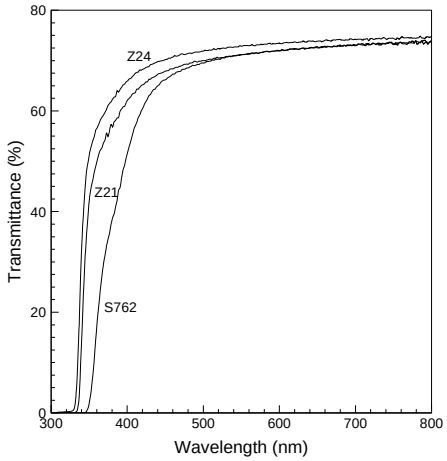

Figure 9: Longitudinal transmittance for samples Z24, Z21 and S762.

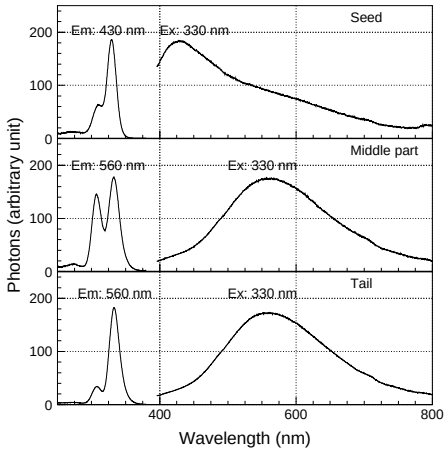

Figure 10: Photo luminescence measured at three positions along the axis of sample Z9.

6 Longitudinal Uniformity

One important technical issue for doping is the uniformity. Since the segregation coefficient of a dopant in $PbWO_4$ crystals is usually not equal to one, the dopant tends to distribute not uniformly in the crystal. This would in turn cuase bad longitudinal uniformity for large size samples. This bad longitudinal uniformity, if beyond some limit, may affect calorimeter performance. Our measurement shows that both dopants A and B are not uniformly distributed in $PbWO_4$. Table 2 shows that all A doped samples provide significant more slow component when the seed end is coupled to the PMT, while it is the tail end coupled to the PMT for the B doped samples. This indicates that the dopant A is concentrated at the tail end, and dopant B is concentrated at the seed end. In other words, the segregation coefficient of dopant A in $PbWO_4$ is less than one, and that of dopant B is larger than one.

To study longtitudinal doping uniformity a sample Z9 was grown to 22 radiation length with dopant A in the melt. The spectra of the photo luminescence, decay kinetics and transverse transmittance along the longitudinal axis of the sample Z9 are shown in Figures 10, 11 and 12.

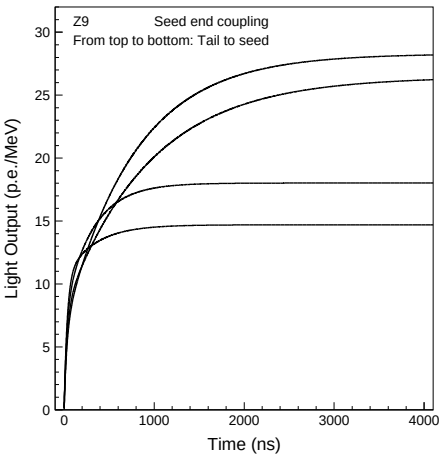

Figure 11: Decay kinetics measured at four positions along the axis of sample Z9.

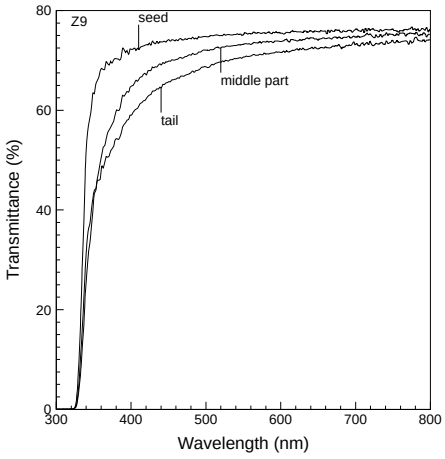

Figure 12: Transverse transmittance measured at three positions along the axis of sample Z9.

Figure 10 shows the exitation (left) and photo luminescence (right) spectra mea-

sured at the seed, middle and tail end of sample Z9. While the emission has both blue and green component at the seed end, it is pure green at the tail end. This is consistent with the segregation coefficient of less than one for dopant A in $PbWO_4$.

The same conclusion can be drawn in decay kinetics measurement. Figure 11 shows that the light from the seed part of the sample has very little slow component, and that from the tail end has significant slow component.

The transverse transmittance can also be used to judge sample longitudinal uniformity. Figure 12 shows good transverse transmittance at the seed end degrades to the tail end of the sample. Although this kind of degradation is sort of expected in Brigman method since all melt goes to the ingot, leading to a relatively large fraction of impurities in the tail end, the difference in the transmittance can be further reduced by defining growth parameters. An alternative solution of this problem is to grow longer ingots and cut off a longer tail part, which, however, would increase the cost.

Similarly, measurements on B doped sample confirms that the segregation coefficient of dopant B is larger than one, causing more green light and more slow component at the seed end.

7 Summary

In the last two years SIC has made an effort in developing new types of $PbWO_4$ crystals with high light yield. It is encouraging to find both dopant A and B are effecive in increasing $PbWO_4$ light output, and up to ten folds of light output increase is observed for these samples as compared to that of the standard Y doped CMS sample. We, however, have not be able to observe a dopant which cause significantly more fast component. This increase of slow component is encouraging for users in high energy and nuclear physics field, but may still fall short for medical applications.

Both A and B doppings cause bad longitudinal uniformity. One interesting approach thus is to double dope $PbWO_4$ crystals with both A and B. Since these two dopants have similar function but with rather different segregation coefficients, it is hoped that they would compesate each other and make large size, longitudianally uniform crystals. When this is achieved, we will have a new type of $PbWO_4$ crystals for high energy and nuclear physics community.

8 Acknowledgments

Work at Caltech is supported in part by U.S. Department of Energy Grant No. DE-FG03-92-ER40701, and at BNL in part by U.S. Department of Energy Contract No. DE-AC02-CH7600016.

References

1. Z.Y. Wei *et al.*, *Nucl. Instr. and Meth.* **A297**, 163 (1990).
2. R.Y. Zhu, *IEEE Trans. Nucl. Sci.* **NS-44**, 468 (1997).
3. P. Lecoq *et al.*, *Nucl. Instr. and Meth.* **A365**, 291 (1995).
4. M. Kobayashi *et al.*, *Nucl. Instr. and Meth.* **A399**, 261 (1997).
5. M. Kobayashi *et al.*, *Nucl. Instr. and Meth.* **A404**, 109 (1998).
6. S. Baccaro *et al.*, *Phys. Stat. Sol.* **A164**, R9 (1997).
7. E. Auffray *et al.*, *Nucl. Instr. and Meth.* **A402**, 75 (1998).
8. M. Kobayashi *et al.*, *Nucl. Instr. and Meth.* **A373**, 333 (1996).
9. R.Y. Zhu *et al.*, *Nucl. Instr. and Meth.* **A376**, 319 (1996).
10. R.Y. Zhu, in *Proceedings of NLC Detector Workshop*, Keystone, Colorado, September 1998; R.Y. Zhu, in *Proceedings of International Workshop on Linear Collider*, Sitges, Barcelona, Spain, May 1999; and in *Proceedings of VIII International Conference on Calorimetry in High Energy Physics*, ed. G. Barreira *et al.*, World Scientific, 226 (1999).
11. P. Lecoq *et al.*, in *Proceedings of IEEE NSS/MIC*, Seattle, November 1999, and A. Annenkov *et al.*, *Nucl. Instr. and Meth.* **A450**, 71 (2000).
12. Powder diffraction data file No. 19-708, JCPDS-ICDD, 1601 Park Lane, Swarthmore, PA 19081, USA, 222 (1979).
13. R.Y. Zhu, *Nucl. Instr. and Meth.* **A340**, 442 (1994).